Surface & Coatings Technology 205 (2011) 3235–3244

Contents lists available at ScienceDirect

Surface & Coatings Technology

journal homepage: www.elsevier.com/locate/surfcoat

Novel hybrid organo-silicate corrosion resistant coatings based on hyperbranched polymers

E. Roussi [a], A. Tsetsekou [a,*], D. Tsiourvas [b], A. Karantonis [c]

[a] School of Mining Engineering and Metallurgy, National Technical University of Athens, 9 Iroon Polytechniou, Zografou Campus, 15780 Athens, Greece
[b] National Centre for Scientific Research "Demokritos", Institute of Physical Chemistry, Agia Paraskevi, 15310 Athens, Greece
[c] School of Chemical Engineering, National Technical University of Athens, 9 Iroon Polytechniou, Zografou Campus, 15780 Athens, Greece

ARTICLE INFO

Article history:
Received 18 June 2010
Accepted in revised form 16 November 2010
Available online 25 November 2010

Keywords:
Corrosion
Coatings
Dendritic polymers
Sol–gel
Aluminum alloy
AA2024-T3 alloy

ABSTRACT

Corrosion protective sol–gel coatings were developed on AA2024-T3 through an aqueous sol–gel process (Modified Self-Assembled Nanophase Particle method) which includes in-situ formation of a dense silica network from hydrolyzed 3-glycidoxy-propyltri-methoxysilane and tetraethoxysilane by proper cross-linking. In the present study, hyperbranched poly(ethylene imine) of two different molecular weights was investigated as a cross-linking agent since this polymer is able to solubilize non-water-soluble organic molecules. In this respect, two organic corrosion inhibitors (2-mercaptobenzothiazole and 2-mercaptobenzimidazole) were combined with poly(ethylene imine) to induce self healing properties. The as developed coatings were also compared with Si/Zr containing coatings developed by a solvent based sol–gel technique. The potentiodynamic scan and the electrochemical impedance spectroscopy methods were employed to evaluate the corrosion protection performance, whereas the chemical structure, morphology and integrity of the coatings were evaluated by Fourier transformed infrared spectroscopy and scanning electron microscopy studies. Formulations that contain poly(ethylene imine) demonstrate better corrosion barrier properties compared to formulations cross-linked with the simple molecule of diethylenetriamine in all cases and especially when combined with the organic inhibitors.

1. Introduction

Aluminum and especially aluminum alloys suffer from corrosion problems when exposed in an aggressive environment, as the passivating layer of alumina is deteriorated, resulting in pitting corrosion. To create long-wearing aluminum products, the alloys are usually pretreated or coated for adequate corrosion protection. Several methods have been applied for protecting aluminum and aluminum alloys against corrosion. To date, the corrosion protection of aluminum alloys used in aircraft has relied extensively on potent hexavalent chromium compounds, which are included in both surface treatments and organic primers. However, it is recognized that chromates are both highly toxic and carcinogenic [1,2] and are banned under the End of Life Vehicle (ELV) Directive (2000/53/EC) and the Registration, Evaluation and Authorisation of Chemicals (REACH) Regulation (COM(03)644(01)).

The sol–gel process is considered an environmentally safe alternative to chromate surface treatments. Sol–gel inorganic metal oxide coatings have been used as corrosion resistant layers for over a decade. Recently, hybrid sol–gel derived organic–inorganic coatings, combining properties of both ceramic and organic components, are being investigated for use as environmentally compliant anti-corrosive and wear-protective surface treatments on Al alloys. The formation of chemical bonds at the interface between substrate and coating can lead to dense, defect-free and uniform hybrid coatings that achieve excellent adhesion and flexibility [3–10]. Further, due to their hybrid nature, they can show excellent compatibility with the organic primer providing thus a very effective barrier [8,11]. Such inorganic–organic networks are formed through the hydrolysis of alkyl-functionalized alkoxysilanes condensed either in the presence or not of various metal alkoxides [12–15].

A significant advantage of this approach is the ability to functionalize these networks by simply varying the network-forming precursors. Tailoring can improve adhesion, strength, hydrophobicity and chemical resistance. Nevertheless, these coatings can present small defects such as microcracks, pinholes, micropores or areas of low cross-link density, which provide the initial path for the electrolyte uptake into the system and the corrosion onset [8,16]. One way to significantly reduce these defects is reinforcing the coating network through the incorporation of inorganic nanoparticles or fillers [8,10]. In this case, the nanoparticles can be functionalized to promote compatibility with the organic primer and also can act as nanoreservoirs of corrosion inhibitors [10]. Another way to improve the barrier film is to use a multilayer structure. In such a system the

* Corresponding author. Tel.: +30 210 7722213; fax: +30 210 7722119.
E-mail address: athtse@metal.ntua.gr (A. Tsetsekou).

0257-8972/$ – see front matter © 2010 Elsevier B.V. All rights reserved.
doi:10.1016/j.surfcoat.2010.11.037

bottom layer provides adhesion to the substrate and corrosive protection, whereas the top layers, apart from complementing the anti-corrosive properties, provide the necessary compatibility with the primer [16].

The incorporation of corrosion inhibitors into the sol–gel films is however the way which can definitely improve the corrosion protection providing even 'self healing' abilities to the coating. These are compounds that can suppress the corrosion mostly by covering the surface by passive layers and by forming complexes with the substrate alloy [7]. Various types of inorganic or organic inhibitors have been investigated up to now. The inorganic inhibitors include phosphates, vanadates, borates, cerium and molybdenum compounds [17–19]. Among them, cerium salts seem to lead to the more effective and environmentally friendly inhibitors [17]. The solubility and stability of complexed Ce^{4+} in solution, combined with the insolubility of its reduced Ce^{3+} form are factors for its success. Concerning the organic corrosion inhibitors, those most investigated have been nitrogen and sulfur based, the most common being azoles (triazoles and thiazoles) [12]. The ability of these organics to bind to corrosive chloride ions has led to their popularity for corrosion protection. However, it has been observed that the inhibitors when they are occluded in free form in the sol–gel matrix have a negative effect on the stability of the protective film [17].

Therefore, the way of incorporation of the inhibitor into the system is a significant parameter. For this purpose, very recently, the research efforts focus on encapsulating, complexating or isolating the inhibitor in suitable nanoreservoirs in order to avoid the direct interaction with the sol–gel matrix and to also achieve its slow release. This is tried through its inclusion in nanoparticles [20,21], its encapsulation using a layer by layer approach [17] or its complexation with other molecules such as β-cyclodextrin [22,23].

Another issue is, however, that most of the sol–gel systems that are developed, are alcohol-based failing to meet the strict regulations for volatile organic compound (VOC) restrictions [7]. Therefore, the research efforts are also directed towards the development of water-based systems which result in low volatile organic compound (VOC) content materials and processes. Water-based silane systems however are less effective than alcohol-based ones. The reason is that drying is more complete in the latter due to their high alcohol content. In turn, the removal of more water facilitates the reaction of silanol groups to form a more cross-linked and denser film. Also, the water-based systems remain more hydrophilic even after drying so they are less impervious to water than the solvent based silanes. The proper incorporation of corrosion inhibitors in these systems which can leach out slowly is of great importance [7].

A method of forming functionalized silica nanoparticles in situ, through an aqueous sol–gel process and the subsequent cross-linking of the nanoparticles to form a thin film, was first described by the Air Force Laboratory in the U.S.A. This so-called 'Self-Assembled Nano-Shape Particles' (SNAP) process, and its newer evolution the 'Modified Self-Assembled Nano-Shape Particles' (MSNAP), can be used to form thin, dense, protective surface coatings on Al aerospace alloys by cross-linking the functionalized nanoparticles upon application, using epoxy amine chemistry [24,25] and diethylenetriamine (DETA) as a cross-linking agent. Doping these coatings with corrosion inhibitors (mercaptobenzothiazole — MBT-, mercaptobenziimidazole — MBI-, mercaptobenziimidazole-sulfonate, and thiosalicylic acid) improved sufficiently the corrosion protection properties. Moreover, when MBT and MBI inhibitors were incorporated into the MSNAP film through complexation with the molecule of β-cyclodextrin, the anti-corrosive performance of the coating was even better due to the prolonged release of the inhibitor from β-cyclodextrin–inhibitor complexes [22,23].

In the present work, this amine is replaced by a hyperbranched poly(ethylene imine) polymer (PEI). PEI is a highly branched cationic polymer bearing in its branches secondary and primary amino end groups, therefore resembling the chemical structure of DETA,

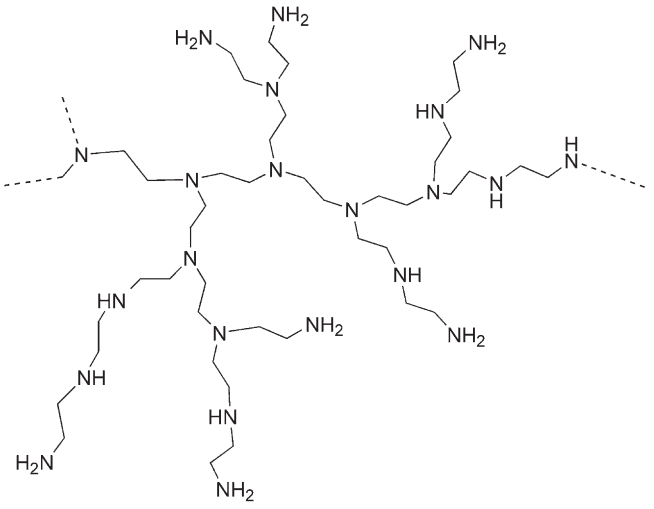

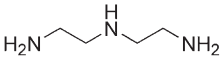

Scheme 1. The chemical structures of PEI and DETA.

(Scheme 1), and is readily available in several molecular weights [26,27]. Due to its chemical structure it can react with epoxides acting as a cross-linking agent for hybrid film formation while, due to its polymeric nature, has also good film forming ability. It possesses anti-corrosive properties by itself [28] and finally, as a hyperbranched polymer, it can encapsulate in its interior non-water-soluble organic molecules [29,30]. In this respect it is envisaged that it can solubilize corrosion inhibitors, such as the non-water-soluble 2-mercaptobenzothiazole (MBT) and 2-mercaptobenzimidazole (MBI), and integrate them into hybrid organo-silicate film coatings.

In this paper we therefore develop an anti-corrosion process based on PEI employing the principles of the MSNAP aqueous sol–gel process. The use of such a macromolecule as a cross-linking agent is compared with that of the simple molecule of diethylenamine (DETA). Two PEI macromolecules differing in their molecular weights are investigated and compared for this purpose, whereas coatings, with or without corrosion inhibitors (MBI and MBT), are developed. The novel water-born PEI-based coatings are also compared with a coating developed by a solvent based sol–gel process involving copolymerization of epoxy silane/zirconium precursors.

2. Experimental

2.1. Development of coatings

AA2024-T3 alloy panel in the form of 60×20×2.45 mm flat coupons was employed for the application of coatings. The nominal composition of this alloy is given in Table 1. The AA2024-T3 coupons

Table 1
Composition of aluminum 2024-T3 alloy.

Element	Cu	Mg	Si	Fe	Mn	Cr	Zn	Ti	Other	Al
wt.%	3.8–4.9	1.2–1.8	0.50	0.50	0.3–0.9	0.10	0.25	0.15	0.15	Balance

were cleaned in an alkaline aqueous solution containing 50 g/l of TURCO TM 4215 (TURCO S.A. SPAIN) for 15 min at 60 °C followed by immersion into a 20% v/v HNO_3 (Merck) solution for 15 min and then rinsed by deionized water. This treatment is applied industrially for AA2024 and leads to partial dissolution of surface intermetallic phases [10].

The coatings were prepared by an aqueous sol–gel method based on the Modified Self-Assembled Nanophase Particle (MSNAP) process [24]. For comparison purposes, solvent based Si/Zr containing coatings were also developed. All kinds of coatings were applied to alloy coupons by exactly the same application procedure. For this purpose, the development, in all cases, involved an optimization stage to identify the optimum synthesis conditions.

In the first case of the aqueous process, the solution was prepared through a drop-wise addition, under continuous stirring, of 3-glycidoxypropyltri-methoxysilane (GPTMS) (97% pure, Merck) and tetraethoxysilane (TEOS) (99% pure, Alfa Aesar) in 3:1 molar ratio to a 0.05 M solution of acetic acid (Merck) in doubly distilled deionized water. The resulting solution (30.4% v/v and 9.4% v/v in GPTMS and TEOS, respectively) was aged at room temperature under stirring for 3 days for the hydrolysis and condensation reactions to take place and then it was further diluted, by a factor of 2, with water. Then, the surfactant (1% v/v Darvan-C, Vanderbilt-USA) and the cross-linking agent were added. For this, either 0.5 ml of diethylenetriamine (DETA) (Merck) or 0.7 g of the hyperbranched polymer poly(ethylene imine) (PEI) was added in 20 ml solution. Two PEI polymers differing in their molecular weights (MW) were employed for this purpose: PEI of MW = 5,000 from Hyperpolymers (assigned as PEI5000) and PEI of MW = 25,000 from Aldrich (assigned as PEI25000).

Furthermore, sols containing organic corrosion inhibitors were also prepared with the aim to incorporate them into the hybrid organo-silicate coatings and test their corrosion inhibition. For this, 0.023 g of 2-mercaptobenzothiazole (MBT, Alfa Aesar) or 0.021 g of 2-mercaptobenzimidazole (MBI, Alfa Aesar) was dissolved into 20 ml of the as prepared solution prior to the addition of the cross-linking polymer.

Finally, a dip coating process was employed to coat the aluminum alloy 2024-T3 coupons involving their dipping into the final sol (immediately after its preparation) for 300 s followed by controlled ascension with a speed of 10 cm/min and curing at room temperature for 24 h. The coatings developed by this way are summarized in Table 2.

The Si/Zr sol–gel process involved the preparation and mixing of two different sols: an organosiloxane one and a second alcosol that served as a source of hydrolyzable zirconium. The organosiloxane sol was prepared by mixing the GPTMS and TEOS precursors with 2-propanol (Merck) in a 1:4:5 volume ratio. The resulting solution was kept under continuous stirring at room temperature for 30 min. The second alcosol was prepared by adding ethylacetoacetate (Merck) in a solution (70% v/v) of tetra-n-propoxyzirconium (TPOZ) in n-propanol (Alfa Aesar) in a 1:1.5 volume ratio. This solution was kept under stirring at 60 °C for 3 h. Then, the two sols were mixed in a Zr/Si atomic ratio of 1:4 (~20 mol% ZrO_2) and the as formed sol was further stirred for 60 min and aged for another 1 h at room temperature. Finally, the same dip coating process as described earlier (involving dipping of substrates into sol for 300 s followed by controlled ascension) was employed to coat the alloy coupons. Drying at 100 °C for 1 h followed in this case. The coatings developed by this way are denoted as Si/Zr sol–gel.

Table 2
Coatings prepared.

Coating code	Cross linking agent	Organic inhibitor
Si/Zr sol–gel	–	–
DETA	DETA	–
PEI5000	PEI5000	–
PEI25000	PEI25000	–
DETA-MBI	DETA	MBI
PEI5000-MBI	PEI5000	MBI
PEI25000-MBI	PEI25000	MBI
DETA-MBT	DETA	MBT
PEI5000-MBT	PEI5000	MBT
PEI25000-MBT	PEI25000	MBT

2.2. Characterization of coatings

The corrosion behavior of the coated aluminum specimens was examined through potentiodynamic scan (PDS) measurements conducted in Harrison's solution (0.35 wt.% $(NH_4)_2SO_4$ and 0.05 wt. % NaCl) with the aid of a Potentiostat/Galvanostat Model 263A (EG&G, Princeton Applied Research, instrumentation accuracy ± 5 nA). The Harrison's solution emulates the atmospheric conditions of an aircraft in great detail [31]. Electrochemical measurements were executed using a one-chamber, three-electrode cell. The reference electrode was a Ag/AgCl electrode connected through a Luggin capillary, whereas the cathode was a platinum electrode. The experiments were carried out at 20 °C employing a scan rate of 0.2 mV/s and each coating system was evaluated in triplicate. Before polarization is applied, the samples were immersed in the solution for a period of 90 min. The Tafel plots were statistically fitted to the Stearn–Geary model for a corroding system by using the Power Corr Software.

The corrosion behavior of the coated substrates was also determined by electrochemical impedance spectroscopy (EIS). The EIS measurements were accomplished using a Solarton SI 1260, impedance/Gain-phase analyzer. These measurements were performed at room temperature using a three-electrode electrochemical cell, consisting of the working electrode (1 cm^2 area), saturated calomel electrode (SCE) as reference and platinum as counter electrode. The measuring frequency ranged from 10^5 Hz down to 10^{-2} Hz. The r.m.s. voltage was 10 mV. The EIS experiments initially were performed after immersion of the coated substrates in Harrison's solution for 72 h. Spectra were treated using the Software Zplot/Z-view (Scribner Assoc. Inc.).

Further, scanning electron microscopy (SEM) studies performed in a JEOL JSM 6380-LV instrument were employed to evaluate the surface morphology and quality of the films developed before and after the corrosion tests.

Finally, the chemical structure of the coatings either before or after corrosion was investigated by infrared studies performed using a Nicolet 6700 Fourier Transformed Infrared spectrometer equipped with an Attenuated Total Reflectance accessory (ATR) with diamond crystal (Smart Orbit™, Thermo Electron Corporation). Coated alloy samples were firmly pressed against the diamond and spectra were recorded at 4 cm^{-1} resolution. A minimum of 64 scans were collected and signal averaged.

Attenuated total reflection (ATR) is a method of choice for the analysis of the surface of materials and for the characterization of materials that are opaque or too thick to be analyzed by normal infrared spectroscopy recorded by passing a beam of infrared light through the sample. In this technique the sample surface is firmly pressed to come into direct contact with the surface of an optically dense crystal, in this case a diamond crystal. The beam of infrared light is passed through the crystal so that it is totally reflected, at least once, off the surface which is in contact with the sample. ATR sampling technique operates by measuring changes in absorbance of specific frequencies in the totally internally reflected infrared beam after the beam comes in contact with the sample. The beam is collected by the detector as it exits the crystal and the results can be presented either as absorbance or transmittance IR spectra.

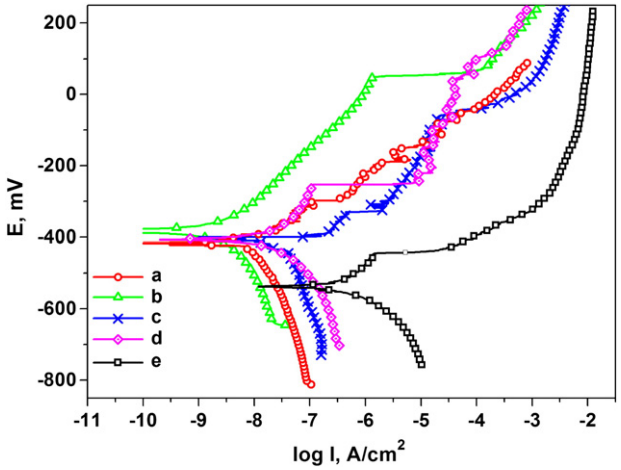

Fig. 1. Potentiodynamic scans of AA2024 alloy in Harrison's solution: a) PEI5000, b) PEI25000, c) DETA, d) Si/Zr sol–gel coated samples and e) bare sample.

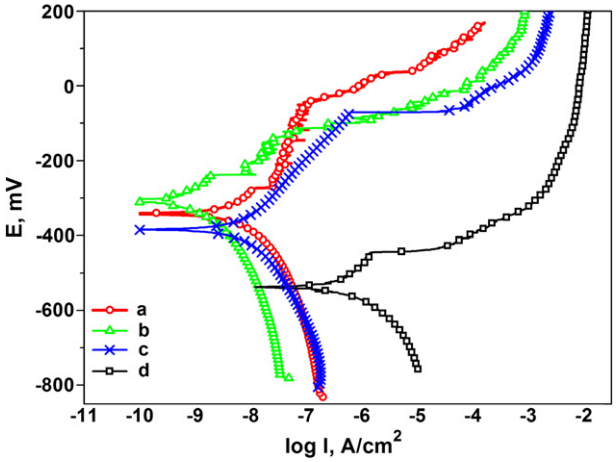

Fig. 3. Potentiodynamic scans of AA2024 alloy in Harrison's solution: a) PEI5000-MBT, b) PEI25000-MBT, c) DETA-MBT coated samples and d) bare sample.

3. Results and discussion

3.1. Corrosion resistance of coatings

PDS measurements were used to evaluate the corrosion resistance of different coatings on AA2024-T3 substrate. Figs. 1–3 show representative potentiodynamic polarization curves of bare and coated AA2024-T3 substrates in Harrison's solution. The corrosion parameters, as determined by Tafel analysis of the PDS data, i.e. corrosion potential (E_{corr}), corrosion current density (i_{corr}) and corrosion rate (mpy — mils per year penetration) are recorded in Table 3. The results clearly demonstrate the corrosion barrier properties of the coatings applied.

Fig. 1 depicts the polarization curves of coated AA2024-T3 specimens, not incorporating corrosion inhibitors, together with the respective curve of bare Al alloy. As can be easily seen, the polarization curves of coated specimens shift to a more positive potential and lower current density values in comparison to bare alloy indicating the protection of the substrate against corrosion. This is reflected on the values in Table 3, where it is clearly observed that E_{corr} for coated Al alloy specimens are considerably higher than the respective value for bare alloy. Further, the values of i_{corr} for coated alloy specimens are in the order of a few nA/cm^2, i.e. about two orders of magnitude lower than that of bare specimen. Among the different coating formulations applied, the E_{corr} values do not differ significantly; however, comparing the i_{corr} values, it is seen that the PEI cross-linked formulations show the lowest values. In contrast, DETA coating presents the highest i_{corr} values, thus, offering less protection in comparison to all other types of inhibitor-free coatings.

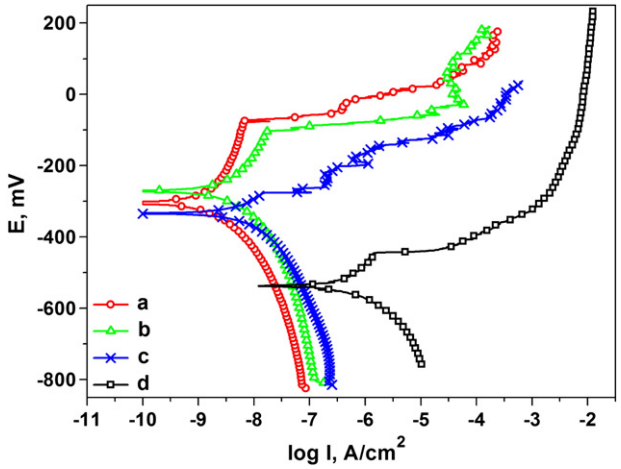

Fig. 2. Potentiodynamic scans of AA2024 alloy in Harrison's solution: a) PEI5000-MBI, b) PEI25000-MBI, c) DETA-MBI coated samples and d) bare sample.

The polarization curves of coated AA2024-T3 specimens incorporating MBI inhibitor are presented in Fig. 2. These curves shift to more positive E_{corr} potential and to lower current density values, in relation to the curves obtained for both bare Al alloy and inhibitor-free coated specimens, indicating the improved protecting action of this kind of coatings. Among them, the coatings cross-linked with PEI behave more effectively as they present better defined passivation regions compared to the DETA-MBI coating. Furthermore, by inspecting the values of E_{corr} shown in Table 3, it is observed that the differences among coatings incorporating the MBI inhibitor are rather small, but a considerable positive shift is observed for the corrosion potential of this type of coatings in comparison with MBI-free coatings. A similar conclusion is derived by inspecting the i_{corr} values for coatings containing MBI (Table 3). The values of i_{corr} are very small in comparison to bare Al alloy and considerably smaller than those obtained for specimens with inhibitor-free coatings. Thus, better performance is observed when MBI is present in the coating, whereas PEI–MBI coatings exhibit the best protection against corrosion.

The effect of incorporating MBT inhibitor in the coating is presented in Fig. 3 where the PDS curves of the respective specimens are shown together with the curve of bare Al alloy. The behavior of these coatings is similar to those incorporating MBI inhibitors. In this case as well, the PEI cross-linked formulations present better barrier properties compared to the DETA-MBT coating.

Overall, PDS measurements indicate that PEI coatings, either with or without inhibitors exhibit very low corrosion current densities thus offering very good protection against corrosion. Among them, those including inhibitors show the most positive shift of E_{corr} values and

Table 3
PDS results for coatings.

Sample	i_{corr} (nA/cm^2)	Corrosion rate (mpy)	E_{corr} (mV)
Al untreated	486	0.21	−537
Si/Zr Sol–gel	36	0.015	−406
DETA	92	0.04	−409
PEI5000	15	0.007	−413
PEI25000	6	0.003	−380
DETA-MBI	18	0.008	−334
PEI5000-MBI	1	0.00044	−298
PEI25000-MBI	8	0.0035	−271
DETA-MBT	20	0.0088	−384
PEI5000-MBT	10	0.0044	−341
PEI25000-MBT	1	0.00044	−297

the lowest i_{corr} values. The enhanced behavior of these coatings can be justified by the effective incorporation of the corrosion inhibitor (MBT or MBI) into the coating layer [17] due to the solubilization properties of PEI. Indeed, while MBT and MBI are practically water insoluble (<0.1 mg/ml and ~0.2 mg/ml for MBT and MBI respectively), their solubilities in PEI solutions employed in this study (0.07 g/ml) are substantially increased. MBT solubility is 31.5 and 32.9 mg/ml in PEI5000 and PEI25000 solutions respectively, while MBI solubility is 4.1 and 6.5 mg/ml in PEI5000 and PEI25000 solutions respectively. On the other hand, DETA coatings exhibit the highest corrosion current density values, whereas the respective values of DETA-MBI and DETA-MBT coatings remain higher than those of PEI5000 and PEI25000 formulations, suggesting similar or even worse barrier performance compared to these inhibitor-free PEI formulations. However, the corrosion potential of all coatings is significantly higher than that of bare Al alloy, indicating their ability to inhibit the anodic process by acting as barriers and thus impeding the contact of the electrolyte with the metal surface.

EIS data of Al alloy substrates coated with sol–gel, PEI or DETA cross-linked coatings after their immersion in Harrison's solution for 72 h are presented in Figs. 4–6. In order to interpret the EIS data it is assumed that the system consists of three interfaces with different resistance and capacitance characteristics: a) the electrolyte penetrates the coating through its pores which exhibit the pore resistance; b) on the metal substrate an additional layer exists due to the oxide formation; and c) moreover, on the metal surface the corrosion reactions proceed. Thus, in this system three different time-scales are

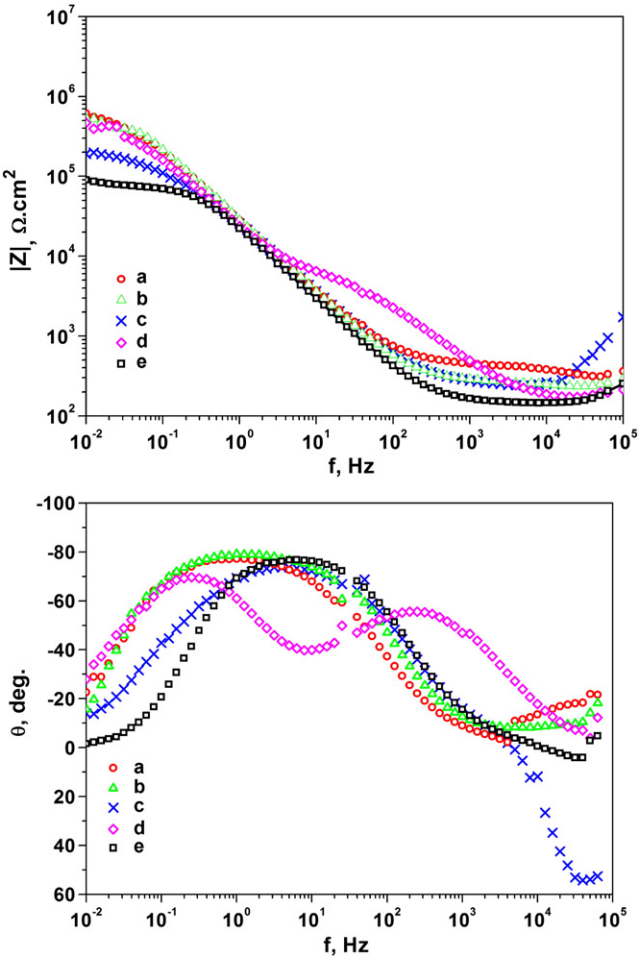

Fig. 4. Bode plots of AA 2024 aluminum alloy after 72 h of immersion in Harrison's solution: a) PEI5000, b) PEI25000, c) DETA, d) Si/Zr sol–gel coated samples and e) bare sample. Zmod is an impedance module.

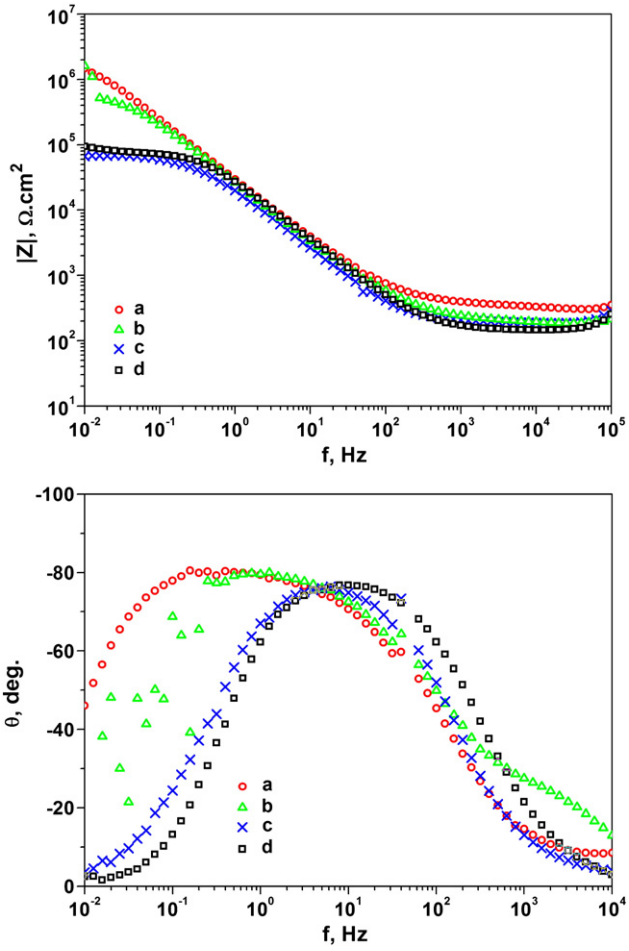

Fig. 5. Bode plots of AA 2024 aluminum alloy after 72 h of immersion in Harrison's solution: a) PEI5000-MBI, b) PEI25000-MBI, c) DETA-MBI coated samples and d) bare sample.

expected to be observed due to the existence of the three different interfaces. In principle, for very high values of frequency, the solution (bulk) resistance as well as the capacitance of the coating are expected to be observed, whereas for intermediate frequencies the pore resistance, oxide capacitance and oxide resistance are to be revealed. Moreover for very small frequency values the response must be determined by the electrochemical double-layer capacitance and the polarization resistance due to the corrosion of the substrate.

Typical EIS Bode plots for bare Al alloy and Al alloy coated with inhibitor-free coatings are presented in Fig. 4 in the frequency range from 10^{-2} to 10^{5} Hz. Overall, the impedance modulus of all coated specimens is higher than that of bare Al alloy, within the selected frequency range, indicating the protecting action of the coatings. The resistive plateau, ranging from approximately 10^{2} to 10^{4} Hz for DETA, PEI25000 and PEI5000 coatings can be attributed to the pore resistance. Apparently, the pore resistance for the latter is greater than the pore resistance of the other two types of coatings, indicating a decrease of porosity [17]. In the low frequency limit, a mixed response is observed, possibly due to the initiation of corrosion and the slight deterioration of the oxide layer. Among the three types of coatings, DETA exhibits the smaller impedance value at the lower frequency limit whereas both PEI5000 and PEI25000 attain higher values. The case of Si/Zr sol–gel coating is the only one where at least two different time-scales are observed in the impedance modulus spectra, its value at the lower frequency range being compatible with the impedance of PEI5000 and PEI25000 coatings.

In Fig. 5, the Bode plots for Al alloy coated with MBI-incorporated inhibitor coatings are presented, together with the respective plot for

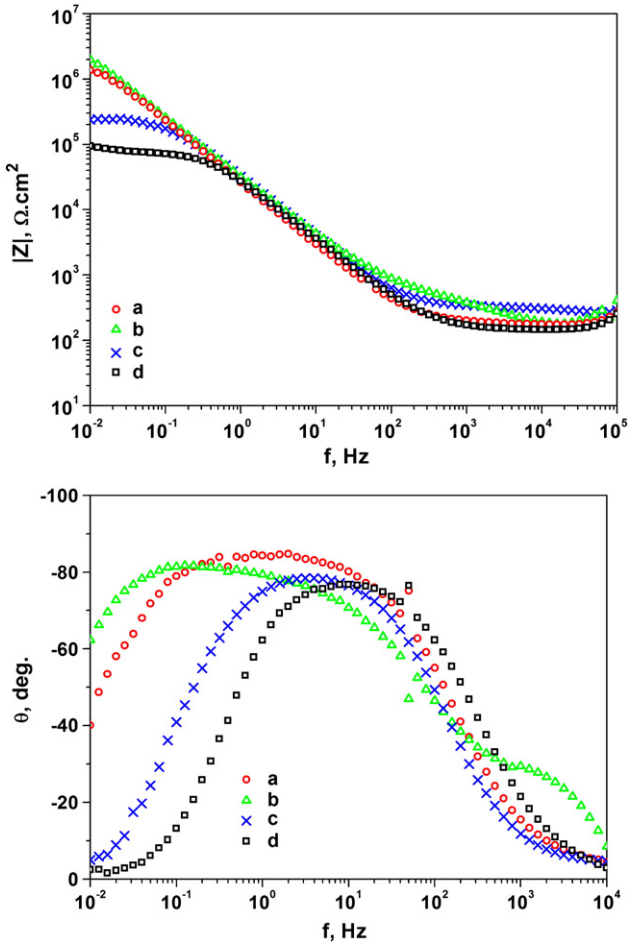

Fig. 6. Bode plots of the AA 2024 aluminum alloy after 72 h of immersion in Harrison's solution: a) PEI5000-MBT, b) PEI25000-MBT, c) DETA-MBT coated samples and d) bare sample.

bare Al alloy. As can be seen, the DETA-MBI coated specimen performs poorly whereas a time constant corresponding to a corrosion process seems to be absent at low frequencies for both PEI5000-MBI and PEI25000-MBI samples (even though the scattered values of the impedance modulus and phase might be an indication of the initiation of corrosion, Fig. 5, curve b). Moreover, comparing the values of the impedance modulus at the low frequency limit between MBI-free and MBI-incorporated PEI coatings (Figs. 4 and 5), it is observed that the protection against corrosion is improved.

Improved protection against corrosion is observed also for coatings containing MBT inhibitor (Fig. 6). As can be seen in this figure, a corrosion process is completely absent within the explored frequency range for PEI5000-MBT and PEI25000-MBT coated specimens. On the other hand, the DETA-MBT coating exhibits a similar frequency response with MBT-free coatings (Fig. 4) both in the high and low frequency ranges, indicating that the presence of the inhibitor does not promote protection against corrosion for this type of coating.

According to Khramov et al. [23], the corrosion protection properties are significantly improved when a corrosion inhibitor is incorporated into the coating matrix. The observed improvement in the case of a coating cross-linked with PEI, may be due to the fact that PEI can solubilize the corrosion inhibitors (MBI and MBT) resulting to the formation of an organo-silicate coating which in addition is in close proximity with the Al surface (see FTIR analysis section). A simple molecule like DETA, on the other hand, does not have these properties and consequently does not offer important improvement.

Zhu and van Ooij [32] explored the corrosion mechanism of bare AA 2024-T3, and they discovered that the corrosion of this alloy starts from the dealloyment of the anodic Al–Cu–Mg-containing intermetallics (Al_2CuMg), followed by a severe cathodic dissolution of the surrounding Al matrix which takes place due to the local alkalization around the intermetallics. More specifically, when the corrosion medium contacts the intermetallic surface, the hydrolysis of Al and Mg leads to the electrochemical evolution of hydrogen, Eqs. (1)–(3), accompanied by oxygen reduction, Eq. (4) [17].

$$2Al + 6H_2O \rightarrow 2Al^{+3} + 6OH^- + 3H_2\uparrow \quad (1)$$

$$Mg + 2H_2O \rightarrow Mg^{+2} + 2OH^- + H_2\uparrow \quad (2)$$

$$2H_2O + 2e^- \rightarrow 2OH^- + H_2\uparrow \quad (3)$$

$$O_2 + 2H_2O + 4e^- \rightarrow 4OH^- \quad (4)$$

The processes of hydrogen evolution and oxygen reduction, result in a local increase of pH [10,17] which can provoke the release of MBT or MBI around the formed defect [17]. In this way, a thin adsorption layer is formed on the damaged metallic surface hindering the expansion of the corrosion phenomena [17].

In order to better understand and elucidate the long term protective properties of the coatings, EIS measurements after 1, 2, 3, 4 and, 8 weeks of immersion in Harrison's solution were also performed. The impedance spectra for Al alloy coated with a PEI5000-MBT incorporated inhibitor, after its immersion in Harrison's solution for the afore mentioned periods, are presented in Fig. 7. The

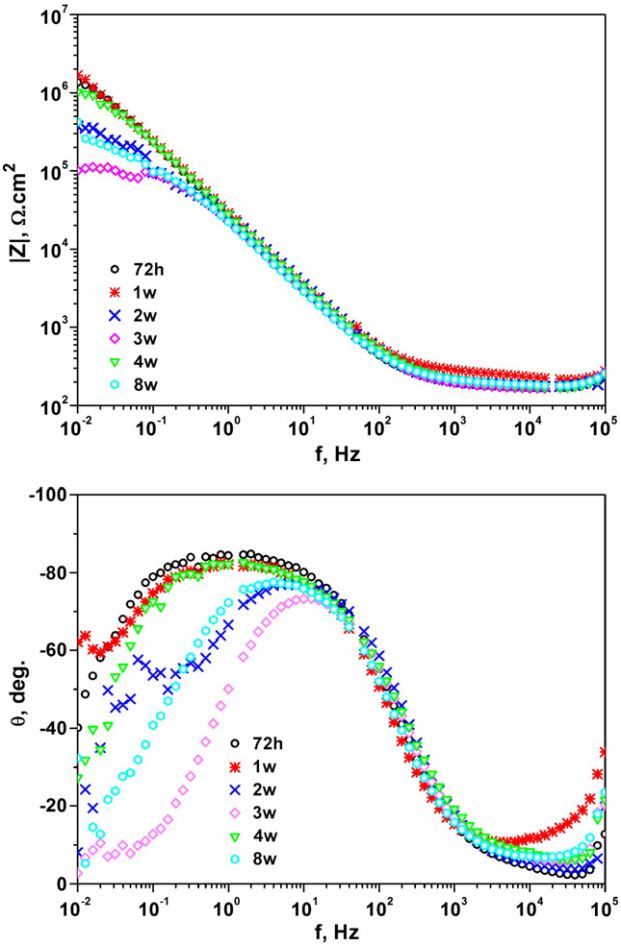

Fig. 7. Bode plots obtained for AA2024 aluminum alloy coated with PEI5000-MBT immersed in Harrison's solution for 72 h, 1, 2, 3, 4 and 8 weeks.

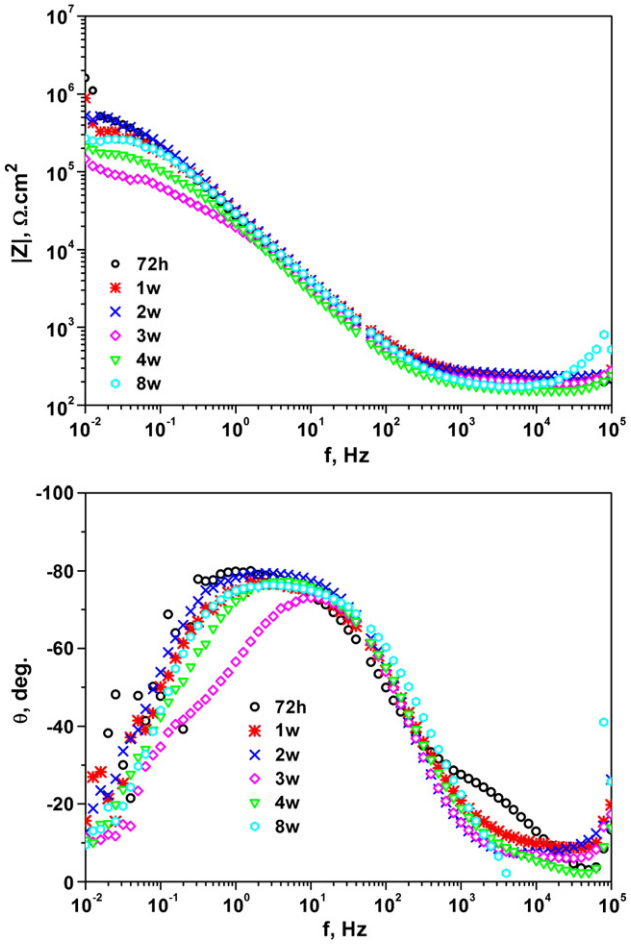

Fig. 8. Bode plots obtained for AA 2024 aluminum alloy coated with PEI25000-MBI immersed in Harrison's solution for 72 h, 1, 2, 3, 4 and 8 weeks.

impedance response in the low frequency region demonstrates a resistance decrease that begins during the 2nd week of immersion, followed by an increase after the 4th week. More specifically, the deterioration of the coating leads to a decreased impedance modulus after the 2nd week (3×10^5 Ω cm^2 in week 2); the impedance modulus decreases further during the 3rd week (1×10^5 Ω cm^2 in week 3). The corrosion inhibitors are most likely released on the damaged area at that time, leading to a significantly increased value of the impedance modulus at the end of the 4th week (1×10^6 Ω cm^2 in week 4); in addition, the impedance modulus retains a high value (higher than the value measured after 3 weeks of immersion) even after 8 weeks of immersion (4×10^5 Ω cm^2 in week 8). Therefore, the results suggest that the anti-corrosive properties of the coated system remain very good even after a 2 month stay in the corrosive solution. Similar behavior is observed in the case of PEI25000-MBI (Fig. 8), the only difference being the fact that its impedance modulus during the 8th week of the experiment retains a slightly higher value than that obtained after 4 weeks of immersion. The surface of the coupon coated with the PEI25000-MBI formulation immediately after its preparation and after the 8 week immersion period in Harrison's solution is shown in Fig. 9. In fact, the treated coupon does not present any corrosion signs on the metal surface, in good agreement with the EIS measurements.

In this respect, it becomes obvious that a combination of inhibitors with PEI promises effective corrosion protection when the coating is placed in an aggressive environment by inducing the self healing of corrosion defects.

3.2. SEM analysis

SEM analysis was employed to evaluate the surface morphology of the coatings before and after corrosion experiments. The scanning electron micrographs before the PDS corrosion test (Fig. 10a and b) verified a good and homogeneous morphology without defects, micropores and crackings in all cases. The thickness of the films is also homogeneous ranging in the order of 2–3 μm (Fig. 10c, d). This morphology is still kept even after the potentiodynamic test, when the scan stops at the breaking potential.

Further, as it can be clearly seen in Fig. 11, picturing the morphology of the coatings after completing the PDS, the films still exist on the surface presenting only small area damages. The extent of the damaged area depends, however, on coating composition. In fact, among the different coatings examined, the lowest number of cracks is clearly observed in the case of PEI–organic inhibitor coating systems (Fig. 11c) which present very few and small microcracks. This result is in good agreement with the corrosion tests which proved these combination PEI–inhibitor formulations as the best performing ones.

3.3. FTIR analysis

Attenuated total reflectance FTIR measurements of PEI5000, PEI25000 and DETA films deposited on Al coupons were employed to study the hydrolysis and condensation reactions of GPTMS and TEOS as well as the reaction between the epoxy group of glycidyl and the amino groups of PEI or DETA thus acting as 'cross-linking' agents. It is well established that hydrolysis and condensation processes of silanes take place near simultaneously [33] under the acidic conditions employed. In addition, after the addition of the 'cross-linking' agent, a ring opening of the epoxy group of GPTMS can either yield

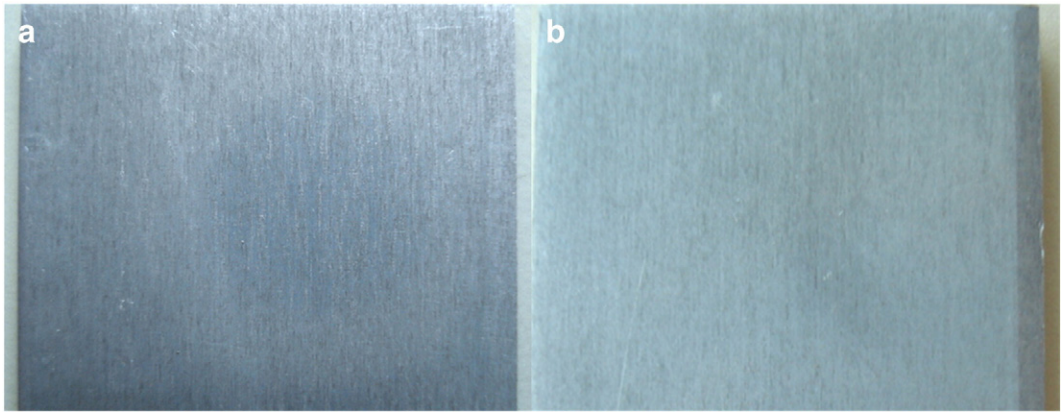

Fig. 9. Optical images of PEI25000-MBI coated sample immediately after preparation (a) and after 8 weeks of immersion in Harrison's solution (b).

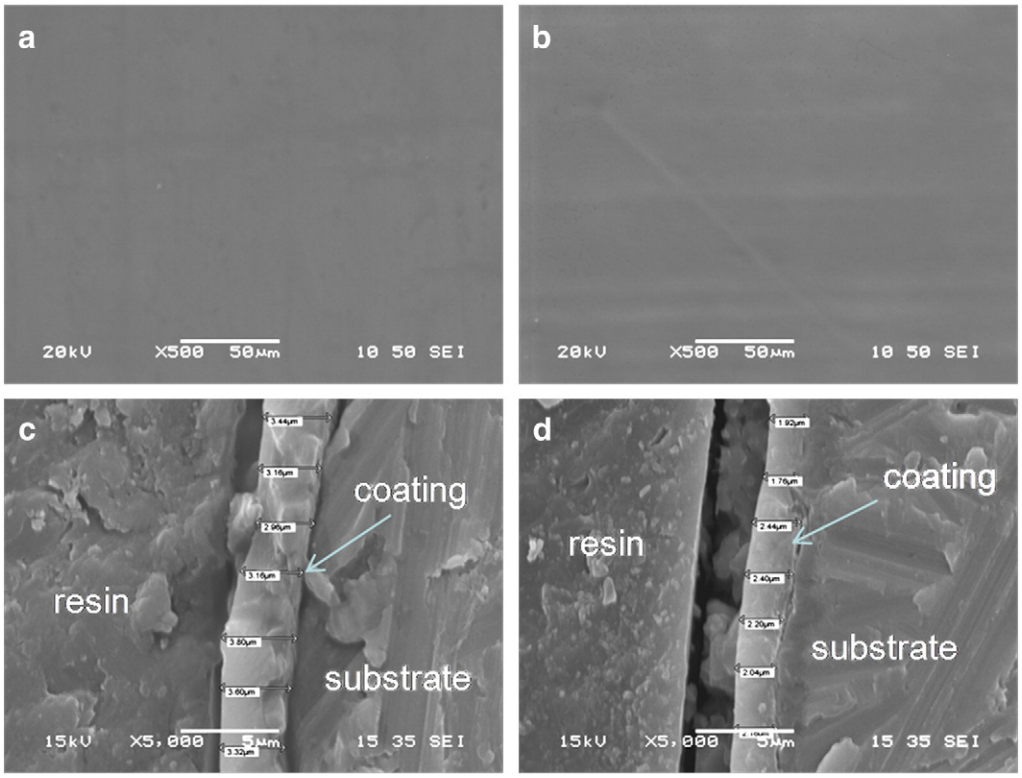

Fig. 10. Scanning secondary electron images of AA2024 coatings before the potentiodynamic (PDS) corrosion test: a) and b) PEI25000 and DETA system, respectively, c) and d) coating–aluminum interface for PEI25000-MBT and Si/Zr sol–gel system, respectively.

primary and secondary alcohol groups (hydrolysis) or react with the primary or secondary amino groups of polyamines that are added to induce 'cross-linking' or film formation.

A broad band in the 3700–3100 cm^{-1} spectral region of PEI25000 or DETA film deposited on Al alloy coupons is related to the presence of OH groups of silanols resulting from hydrolysis of methoxy and

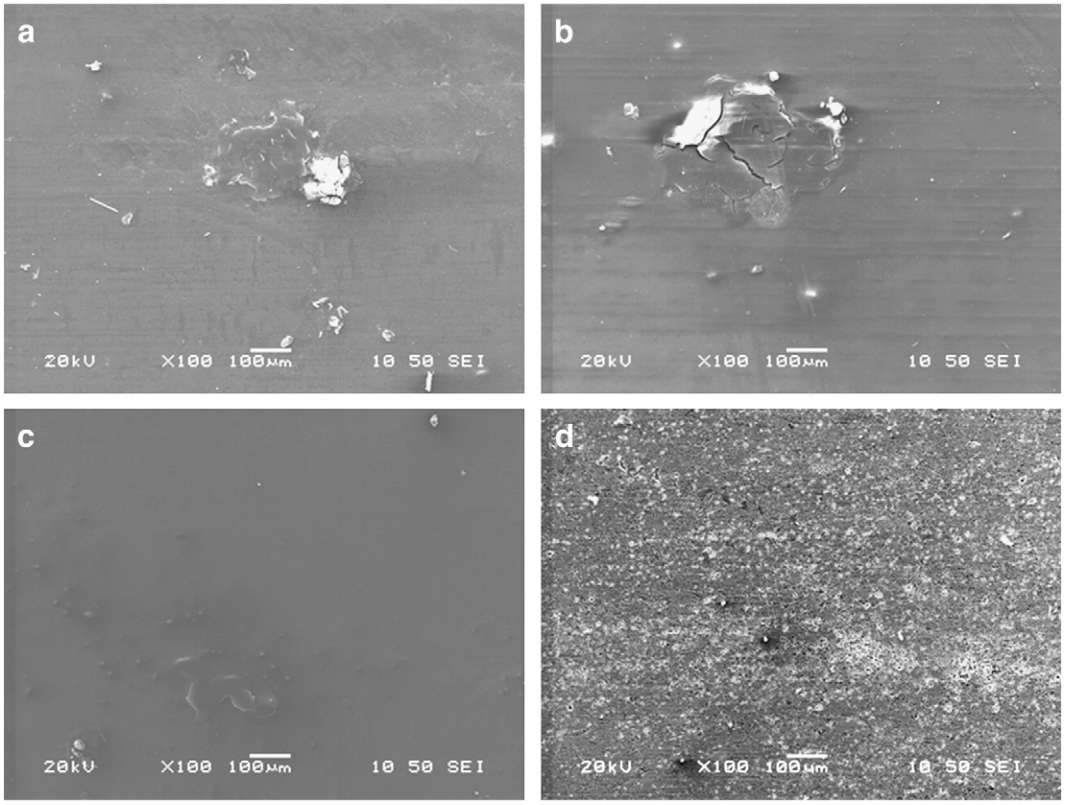

Fig. 11. Scanning secondary electron images of AA2024 coated with a) PEI25000, b) DETA and c) PEI25000-MBT compositions and d) bare Al after the (PDS) corrosion test.

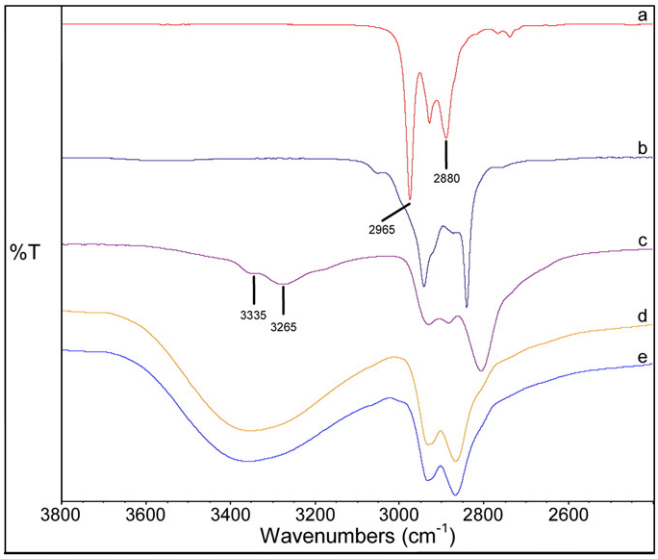

Fig. 12. FTIR spectra of: (a) TEOS, (b) GPTMS, (c) PEI25000 polymer, (d) DETA coating deposited on Al alloy coupons, (e) PEI25000 coating deposited on Al alloy coupons. Spectra were moved along y-axis to improve clarity of presentation.

ethoxy silanes, of the primary and secondary alcohols resulting from epoxy group hydrolysis and in the presence of absorbed water (see also later). As a result, the stretching modes of the primary amino group at 3335 and 3265 cm^{-1} and of the secondary NH groups at 3265 cm^{-1} of either DETA or PEI are hidden beneath the OH band (Fig. 12). This diminishes the utility of this region to follow the ongoing reactions, especially the one between the amine and epoxy groups. However, as also shown in Fig. 12, the absence of the asymmetric (ca. 2965 cm^{-1}) and symmetric (ca. 2880 cm^{-1}) CH_3 stretching modes in the 3000–2800 cm^{-1} region provides evidence for the hydrolysis of methoxysilane and ethoxysilane groups [34].

The characteristic bands [33] originating from Si–O–Si stretching vibrations dominate the 1200–900 cm^{-1} region (Fig. 13). Specifically, the bands at 1150 cm^{-1} (shoulder) and 1200 cm^{-1} are assigned to the longitudinal optic (LO) modes of Si–O–Si bonds and could so be attributed to the development of cross-linked structures forming the silica network. The intense bands at 1085 and 1030 cm^{-1} are assigned to transverse-optical (TO) modes of Si–O–Si bonds present, respectively, in cyclic structures as in vitreous silica or in the dense silica network, and in smaller siloxane rings with larger Si–O–Si angles and Si–O bond lengths present in the sol. Although these bands are subjected to interference from the C–O–C ether band of GPTMS at ca 1100 cm^{-1} and the OH deformation bands of the primary and secondary alcohols at ~1050 and 1100 cm^{-1}, respectively, resulting from the hydrolysis of the epoxy group, it is possible to distinguish the LO bands related to the porous structure of the matrix and the TO bands corresponding to dense silica verifying the condensation reactions of silanes. Finally, whereas the band at 950 cm^{-1} corresponding to the stretching vibrations of the Si–OH groups is not evident in the spectra, the band at 915 cm^{-1} attributed to the stretching modes of Si–O– is clearly detectable.

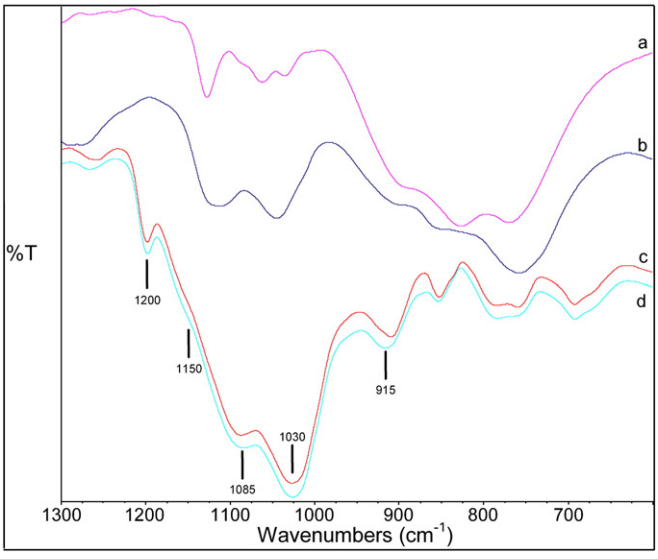

Fig. 13. FTIR spectra of: (a) DETA, (b) PEI25000 polymer, (c) PEI25000 coating deposited on Al coupons, (d) DETA coating deposited on Al coupons. Spectra were moved along y-axis to improve clarity of presentation.

The reaction of the epoxide with amines after three days of aging in the GPTMS–TEOS solution necessitates, at first, the verification that epoxy groups are still present in the solution, since it is known that acidic conditions accelerate the ring opening [35]. Indeed, the epoxy ring C–O stretching vibration at 1254 cm^{-1} is present in the FTIR spectra of the solutions aged for 3 days and is comparable in intensity to the band of the same solution obtained immediately after preparation. Interestingly, after coating Al specimens with this solution, i.e. without adding any amine, the resulting film after drying does not exhibit this vibration band in its spectrum (Fig. 14); apparently the epoxide ring opening is catalyzed by the Lewis acid active surface groups of Al specimens. Epoxy groups are therefore available to react with amine groups in solution and this reaction is catalyzed and completed on the Al surface.

The reaction is further followed by monitoring spectral changes in the 1750–1500 cm^{-1} region containing bands originating from the amino groups of the 'cross-linking agents'. The NH_2 deformation mode of the primary amino groups of both DETA and PEI at 1600 cm^{-1} (Fig. 14) is no longer detectable in the spectra of organo-silicate hybrid coatings whereas new bands appear at 1735, 1720 and at 1562 cm^{-1}. An additional band at 1645 cm^{-1} is attributed to the bending vibration of water molecules absorbed on silica gel [36]. The absence of the 1600 cm^{-1} band indirectly indicates the reaction of primary amino groups with epoxides affording secondary amino groups; the respective deformation mode in secondary amines is extremely

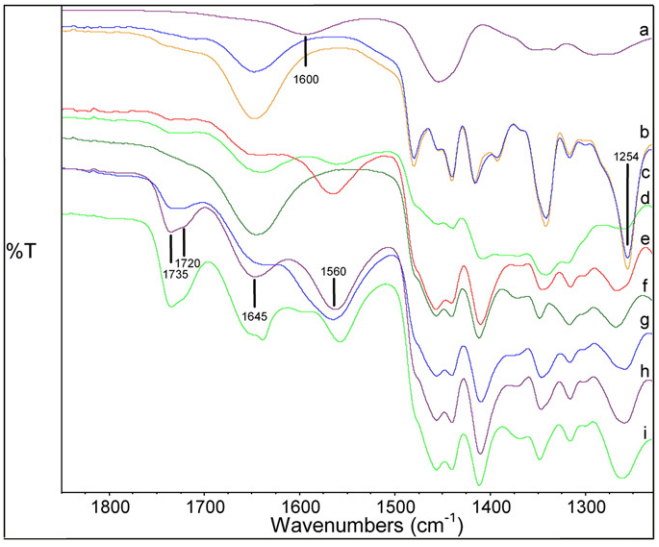

Fig. 14. FTIR spectra of: (a) PEI25000 polymer, (b) SNAP solution after 3 days of aging, (c) SNAP solution immediately after preparation, (d) SNAP solution after addition of PEI and subsequent drying, (e) PEI25000 coating deposited on Ti coupons, (f) SNAP solution (no polyamine added) deposited on Al coupons, (g) PEI25000 coating deposited on Al alloy coupons treated with HNO_3, (h) PEI25000 coating deposited on Al alloy coupons that have not been treated with HNO_3, (i) PEI25000 coating deposited on Al alloy coupons after being subjected to potentiodynamic corrosion experiments. Spectra were moved along y-axis to improve clarity of presentation.

weak and practically not detectable in their IR spectra [37]. The new band observed at 1560 cm^{-1} can be assigned to NH deformation modes of amino groups either hydrogen-bonded to SiOH groups, as suggested in the case of amine derivatives absorbed on silica or glass [38,39], or interacting with the Lewis acid sites of alumina, as suggested for butylamine absorbed on alumina [40]. Both assignments can be valid in our case since a) this band is considerably stronger in the case of HNO_3 treated Al specimens (Fig. 14, curve g) and b) the band is present, but lower in intensity, in PEI cross-linked films deposited on Ti where NH groups can only form hydrogen bonds with SiOH groups (Fig. 14, curve e). Overall therefore, the film is 'cross-linked' and stably attached on Al coupons both through covalent bond formation and non-covalent, but rather strong [40], interactions of amino groups with silica and alumina active sites.

The bands at 1720 and 1735 cm^{-1} are tentatively assigned to the acid and ester groups of oxidation by-products of PEI. It has recently been established that branched polyamines such as poly(amido amine) or poly(propylene amine) dendrimers are oxidized in air or after aging their water solutions at pH 8 and below [41]. As discussed in detail in the literature [42], under such conditions carboxyl groups are formed resulting from the oxidation of primary amines and also from chain cleavage. This leads to amide as well as to un-ionized and ionized carboxyl group formation that result via nitrone and oxazirane intermediates. It is therefore of special interest to follow PEI oxidation since it is directly related to the anti-corrosive properties of the coatings. PEI is not oxidized during sol–gel hydrolysis–condensation and subsequent cross-linking as shown by the spectra of dried PEI cross-linked film (Fig. 14, curve d). Oxidation of PEI is favored at low pH values [41] and, in addition, the whole process during which cross-linking occurs is considerably short in time for oxidation species to be observed during solution preparation and film formation. Additionally, the oxidation bands at 1720 and 1735 cm^{-1} are present but less intense (Fig. 14, curve e) in PEI cross-linked coatings applied on Ti coupons compared to the same coatings applied to pure Aluminum foil (data not shown) or to Aluminum AA 2024-T3 alloy (Fig. 14, curve h). Furthermore, upon subjecting the coated Al coupons to potentiodynamic corrosion experiments these bands further increase in intensity (Fig. 14, curve i). It is therefore clear that PEI deposited on Al surfaces is partially oxidized, and oxidation continues upon application of oxidative stresses. In this way, it does not only act as a cross-linking agent for hybrid film formation, as an effective 'binder' to Al surfaces or as a solubilizer of organic corrosion inhibitors, but also as a corrosion inhibitor by itself contributing in a variety of ways to the overall properties of the hybrid film. In this context it should be noted that the corrosion inhibitor effectiveness of PEI for stainless steel reported in the literature [28] supports our results. On the other hand, excessive oxidation damage would result in severe degradation of PEI and therefore loss of its film forming and Aluminum binding properties.

4. Conclusions

Sol–gel derived organo-silicate hybrid coatings prepared using hyperbranched poly(ethylene imine) with or without organic corrosion inhibitors (MBT and MBI) were developed on AA2024-T3 to provide active corrosion protection when the integrity of coating starts to fail. The coatings were developed through an aqueous alkoxysilane-based sol–gel process including in-situ formation of a silica network by cross-linking with hyperbranched poly(ethylene imine) polymer that additionally can render water-soluble the employed corrosion inhibitors. FTIR analysis proved that the film is 'cross-linked' and stably attached on Al coupons both through covalent bond formation and non-covalent, but rather strong, interactions of amino groups with silica and alumina active sites.

Further, it was shown that films containing PEI, even in the absence of corrosion inhibitors, demonstrate better corrosion protection properties compared to formulations containing corrosion inhibitors and employing DETA as a cross-linking agent and comparable or, in some cases, even better properties compared with Si/Zr coatings prepared through a solvent based sol–gel technique. In fact, PEI deposited on Al surfaces is partially oxidized, and oxidation continues upon application of oxidative stresses, thus acting not only as a cross-linking agent for hybrid film formation, and as a solubilizer of organic corrosion inhibitors, but also as a corrosion inhibitor by itself contributing in a variety of ways to the overall properties of the hybrid film.

Moreover, PEI cross-linked coatings with organic corrosion inhibitors exhibit the best anti-corrosion performance attributed to their optimal integration in the film inducing self healing of corrosion defects.

References

[1] IARC Monographs on the Evaluation of Carcinogenic Risk to Humans, vol. 49, International Agency for Research on Cancer, Lyon, 1990.
[2] M.W. Kendig, R.G. Buchheit, Corrosion 59 (2003) 379.
[3] J. Wen, G.L. Wilkes, Chem. Mater. 8 (1996) 1667.
[4] E.P. Bescher, J.D. Mackenzie, J. Sol-Gel Sci. Technol. 26 (2003) 1223.
[5] C. Le Pen, J. Vereecken, J. Appl. Electrochem. 35 (2005) 1303.
[6] M.S. Donley, V.N. Balbyshev, N.N. Voevodin, Prog. Org. Coat. 52 (2005) 34.
[7] V. Palanivel, Y. Huangb, W.J. van Ooij, Prog. Org. Coat. 53 (2005) 153.
[8] M.L. Zheludkevich, I.M. Salvado, M.G.S. Ferreira, J. Mater. Chem. 15 (2005) 5099.
[9] A.M. Cabral, R.G. Duarte, M.F. Montemor, M.G.S. Ferreira, Prog. Org. Coat. 54 (2005) 322.
[10] M.L. Zheludkevich, R. Serra, M.F. Montemor, I.M. Salvado, M.G.S. Ferreira, Surf. Coat. Technol. 200 (2006) 3084.
[11] D. Raps, T. Hack, J. Wehr, M.L. Zheludkevich, A.C. Bastos, M.G.S. Ferreira, O. Nuyken, Corros. Sci. 51 (2009) 1012.
[12] R.L. Twite, G.P. Bierwagen, Prog. Org. Coat. 33 (1998) 91.
[13] K. Blohowiak, K. Osborne, K. Krienke, D. Sekits, Proc. of SAMPE Technical Conference, 28, 1996, p. 440.
[14] T.P. Chou, C.C., G.Z. Cao, J. Sol-Gel Sci. Technol. 26 (2003) 321.
[15] Y. Chen, L. Jin, Y. Xie, J. Sol-Gel Sci. Technol. 13 (1998) 735.
[16] L.M. Palomino, P.H. Suegama, I.V. Aoki, M.F. Montemor, H.G. De Melo, Corros. Sci. 51 (2009) 1238.
[17] D.G. Shchukin, M. Zheludkevich, K. Yasakau, S. Lamaka, M.G.S. Ferreira, H. Möhwald, Adv. Mater. 18 (2006) 1672.
[18] N.N. Voevodin, N.T. Grebasch, W.S. Soto, F.E. Arnold, M.S. Donley, Surf. Coat. Technol. 140 (2001) 24.
[19] A.F. Galio, S.V. Lamaka, M.L. Zheludkevich, L.F.P. Dick, I.L. Müller, M.G.S. Ferreira, Surf. Coat. Technol. 204 (2010) 1479.
[20] S.V. Lamaka, M.L. Zheludkevich, K.A. Yasakau, M.F. Montemor, P. Cecílio, M.G.S. Ferreira, Electrochem. Commun. 8 (2006) 421.
[21] E.V. Skorb, D. Fix, D.V. Andreeva, H. Möhwald, D.G. Shchukin, Adv. Funct. Mater. 19 (2009) 2373.
[22] A.N. Khramov, N.N. Voevodin, V.N. Balbyshev, R.A. Mantz, Thin Solid Films 483 (2005) 191.
[23] A.N. Khramov, N.N. Voevodin, V.N. Balbyshev, M.S. Donley, Thin Solid Films 447 (448) (2004) 549.
[24] M.S. Donley, R.A. Mantz, A.N. Khramov, V.N. Balbyshev, L.S. Kasten, D.J. Gaspar, Prog. Org. Coat. 47 (2003) 401.
[25] N.N. Voevodin, J.W. Kurdziel, R. Mantz, Surf. Coat. Technol. 201 (2006) 1080.
[26] C.R. Dick, G.E. Ham, J. Macromol. Sci. Chem. A, 4 (1970) 1301.
[27] B.E. Rivas, K.E. Geckeler, Adv. Polym. Sci. 102 (1992) 171.
[28] M. Finsgar, S. Fassbender, Nicolini, I. Milosev, Corros. Sci. 51 (2009) 525.
[29] M. Arkas, L. Eleades, C.M. Paleos, D. Tsiourvas, J. Appl. Polym. Sci. 97 (2005) 2299.
[30] M. Arkas, D. Tsiourvas, J. Hazard. Mater. 35 (2009) 170.
[31] R. Twite, S. Balbyshev, G. Bierwagen, Proc. Symp. Environ. Accept. Inh. Coat, Special Publication of the Electrochemical Society, 1997, p. 202.
[32] D. Zhu, W.J. van Ooij, Corros. Sci. 45 (2003) 2163.
[33] N.C. Rosero-Navarro, S.A. Pellice, Y. Castro, M. Aparicio, A. Durán, Surf. Coat. Technol. 203 (2009) 1897.
[34] M. Arkas, D. Tsiourvas, C.M. Paleos, Chem. Mater. 17 (2005) 3439.
[35] J. Gorzynski Smith, Synthesis 8 (1984) 629.
[36] G.D. Chukin, A.I. Apretova, J. Appl. Spectrosc. 50 (1989) 418.
[37] L.J. Bellamy, The Infrared Spectra of Complex Molecules, 3rd Ed. Chapman and Hall, London, 1975.
[38] C.H. Chiang, H. Ishida, J.L. Koenig, J. Colloid Interface Sci. 74 (1980) 396.
[39] I. Shimizu, H. Okabayashi, K. Taga, E. Nishio, C.J. O'Connor, Vibr. Spectrosc. 14 (1997) 113.
[40] T. Moritomo, J. Imai, M. Nagao, J. Phys. Chem. 78 (1974) 704.
[41] D. Wang, T. Imae, M. Miki, J. Colloid Interface Sci. 306 (2007) 222.
[42] H.C. Haas, N.W. Schuler, R.L. Macdonald, J. Polym. Sci. Polym. Chem. 10 (1972) 3143.